

# Dalton Transactions

Accepted Manuscript



This is an *Accepted Manuscript*, which has been through the Royal Society of Chemistry peer review process and has been accepted for publication.

*Accepted Manuscripts* are published online shortly after acceptance, before technical editing, formatting and proof reading. Using this free service, authors can make their results available to the community, in citable form, before we publish the edited article. We will replace this *Accepted Manuscript* with the edited and formatted *Advance Article* as soon as it is available.

You can find more information about *Accepted Manuscripts* in the [Information for Authors](#).

Please note that technical editing may introduce minor changes to the text and/or graphics, which may alter content. The journal's standard [Terms & Conditions](#) and the [Ethical guidelines](#) still apply. In no event shall the Royal Society of Chemistry be held responsible for any errors or omissions in this *Accepted Manuscript* or any consequences arising from the use of any information it contains.

**Acknowledgements**

The acknowledgements come at the end of an article after the conclusions and before the notes and references.

Journal Name

RSC Publishing

ARTICLE

## Reductive Lithium Insertion into B-cation deficient Niobium Perovskite Oxides

Antonio Perejon<sup>a</sup> and Michael A. Hayward<sup>\*a</sup>

Cite this: DOI: 10.1039/x0xx00000x

Received 00th January 2012,  
Accepted 00th January 2012

DOI: 10.1039/x0xx00000x

www.rsc.org/

Reaction between LiH and the  $A_nB_{n-1}O_{3n}$  cation deficient perovskite phases  $Ba_5Nb_4O_{15}$ ,  $Ba_6TiNb_4O_{18}$  and  $Ba_3LaNb_3O_{12}$  proceeds by reductive lithium insertion, leading to the formation of  $Ba_3LiNb_4O_{15}$ ,  $Ba_6LiTiNb_4O_{18}$  and  $Ba_3LaLiNb_3O_{12}$  respectively. During lithium insertion into  $Ba_5Nb_4O_{15}$  and  $Ba_6TiNb_4O_{18}$  the respective *ccchh* and *cccchh* stacking sequences are converted into entirely cubic stacking sequences, while the B-cation vacancy order of the two phases is faithfully converted into Li – Nb or Li – Nb/Ti cation order in the lithiated products. In contrast lithium insertion into  $Ba_3LaNb_3O_{12}$  leads to no gross change in structure, with the inserted lithium cations displacing some of the niobium cations leading to a cation disordered material. Transport measurements indicate semiconducting behaviour consistent with variable range hopping for  $Ba_3LiNb_4O_{15}$  and insulating behaviour for  $Ba_6LiTiNb_4O_{18}$  and  $Ba_3LaLiNb_3O_{12}$ . Detailed analysis of the crystal structure of  $Ba_6LiTiNb_4O_{18}$  suggests crystallographic charge ordering in this phase.

**Introduction**

Complex transition metal oxide phases with  $ABO_3$  perovskite structures have been the subject of intense study due to the diverse array of physical properties they can possess. A particularly striking feature of perovskite oxides is their tendency to exhibit correlated electronic behaviour, in which strong interactions between electrons in partially occupied transition metal d-states result in collective behaviour and emergent properties such as superconductivity<sup>1</sup> or colossal magnetoresistance.<sup>2</sup> The prevalence of such correlated electronic behaviour in perovskite phases can be attributed to the network of apex-linked  $BO_6$  octahedra, that make up the perovskite framework, positioning and orienting the octahedrally coordinated transition metal cations such that strong direct d-orbital overlap ( $t_{2g} - t_{2g}$ ,  $\pi$ -type) or indirect metal-anion-metal orbital interactions ( $e_g - O2p_z - e_g$ ,  $\sigma$ -type or  $t_{2g} - O2p_{x,y} - t_{2g}$ ,  $\pi$ -type) are able to efficiently couple the electronic states on neighbouring metal cations.<sup>3,4</sup>

An additional favourable feature of the perovskite family of structures is an inherent chemical flexibility. Tilting and twisting distortions of the apex-linked array of  $BO_6$  octahedra allow pairs of A and B-cations with a wide range of A:B radius ratios to be accommodated within the extended network. As a result almost all the metals within the transition series can be incorporated into perovskite frameworks. When combined with the ability to accommodate large numbers of anion vacancies within perovskite lattices, this gives chemists a large degree of

latitude to modify and tune desirable physical behaviours in perovskite based materials. Thus in combination we can see that transition metal perovskite oxides adopt a lattice which favours strong inter-cation electronic interactions, whilst being amenable to chemical substitution which allows the facile tuning of the resultant correlated electronic states, making them ideal frameworks to study novel electronic phenomena.

Despite the chemical flexibility inherent to the structure type, transition metal perovskite oxides suffer from the same synthetic restrictions as other transition metal oxides, namely that due to the large energetic barriers to ionic diffusion in the solid state, the synthesis of complex oxides is typically performed at high temperature under conditions which select products on the basis of thermodynamic stability. As a result only the most thermodynamically stable phase, or mixture of phases, can be prepared for a given elemental composition under these conditions. This is a significant restriction as particular transition metal oxidation states and coordination geometries tend to be strongly thermodynamically favoured, precluding the formation of other arrangements, and thus limiting the chemical diversity of the materials formed.

Low temperature topochemical (structure conserving) reactions exploit the differing mobility of species within complex oxide phases to exert some kinetic control over product selection. Under these conditions product phases are selected on the basis of the speed of their formation, rather than their thermodynamic stability, allowing metastable phases to be formed. For example

Dalton Transactions Accepted Manuscript

by exploiting the high mobility of oxide anions compared to metal cations in many perovskite oxides, oxygen can be topochemically deintercalated from thermodynamically stable materials to yield reduced metastable phases containing transition metal centres in novel oxidation states and unusual coordination geometries, such as square-planar  $\text{Ni}^{1+}$ ,  $\text{Co}^{1+}$ ,  $\text{Fe}^{2+}$  or  $\text{Ru}^{2+}$  and even octahedral  $\text{Mn}^{1+}$ ,<sup>5-9</sup> allowing the electronic behaviour of these centres to be studied in extended lattices.

Topochemical anion deintercalation necessarily changes the coordination environment of some or all of the transition metal cations in the host lattice. However it is possible to topochemically reduce transition metal oxide phases, while maintaining the local coordination geometries of cations, via the reductive intercalation of electropositive cations, such as lithium or sodium, which auto-ionize on insertion reducing the metal oxide framework. Thus for example lithium intercalation into rutile structured  $\text{RuO}_2$  or  $\text{MoO}_2$  yields  $\text{Li}_{0.9}\text{RuO}_2$  and  $\text{LiMoO}_2$  respectively, which contain highly unusual, octahedrally coordinated  $\text{Ru}^{3+}$  and  $\text{Mo}^{3+}$  centres in extended oxide frameworks.<sup>10-12</sup>

This chemical approach has not been widely applied to  $\text{ABO}_3$  perovskite oxides because the dense perovskite framework contains no obvious coordination sites for accommodating additional cations. There is however a family of  $\text{A}_n\text{B}_{n-1}\text{O}_{3n}$ , B-cation deficient phases which adopt perovskite type structures, which contain layers of empty octahedral cation coordination sites,<sup>13-15</sup> suggesting they could be reduced by cation intercalation to produce novel, reduced perovskite oxide phases. Here we describe the structural and physical changes which occur on lithium insertion into three members of this series:  $\text{Ba}_5\text{Nb}_4\text{O}_{15}$ ,  $\text{Ba}_6\text{TiNb}_4\text{O}_{18}$  and  $\text{Ba}_3\text{LaTi}_3\text{O}_{12}$ .

## Experimental

### Synthesis of starting materials

Samples of  $\text{Ba}_5\text{Nb}_4\text{O}_{15}$ ,  $\text{Ba}_6\text{TiNb}_4\text{O}_{18}$ ,  $\text{Ba}_3\text{LaNb}_3\text{O}_{12}$ , and  $\text{Ba}_5\text{Ta}_4\text{O}_{15}$  were prepared via high-temperature ceramic synthesis routes. Suitable stoichiometric ratios of  $\text{BaCO}_3$  (99.997%),  $\text{Nb}_2\text{O}_5$  (99.9985% dried at 900°C),  $\text{La}_2\text{O}_3$  (99.999%, dried at 900 °C),  $\text{TiO}_2$  (99.995%) and  $\text{Ta}_2\text{O}_5$  (99.993% dried at 900°C) were ground in an agate pestle and mortar and then heated in air at 1000 °C to decompose the carbonate. The resulting materials were then reground and pressed into 13 mm pellets.  $\text{Ba}_5\text{Nb}_4\text{O}_{15}$  was prepared by heating at 1300 °C for two periods of 24 hours;  $\text{Ba}_6\text{TiNb}_4\text{O}_{18}$  was synthesized by heating at 1250 °C for three periods of 24 hours;  $\text{Ba}_3\text{LaNb}_3\text{O}_{12}$  was synthesized by heating the pellets first at 1200 °C for 20 hours and then at 1350 °C in two periods of 20 hours;  $\text{Ba}_5\text{Ta}_4\text{O}_{15}$  was synthesized by heating at 1100 °C for 24 hours and then at 1150 °C for 24 hours. In all cases single phase products were obtained, confirmed by X-ray powder diffraction, with lattice parameters in good agreement with literature values.<sup>13-16</sup>

### Lithium intercalation

Lithium intercalation was performed using LiH (99.4%). To investigate the reactivity of the oxides with LiH, test reactions were performed on small samples (~400 mg) of the starting materials ground together with 3 molar equivalents of LiH. All manipulations of solids were carried out in a argon-filled recirculating glovebox ( $\text{O}_2$  and  $\text{H}_2\text{O} < 1\text{ppm}$ ). The mixtures were then sealed under vacuum within Pyrex or fused silica tubes, depending on the final reaction temperature, and heated at temperatures between 300°C and 500°C for 3 day periods.

Due to hazards associated with the formation of hydrogen gas when performing reactions with LiH, large samples suitable for neutron powder diffraction analysis were prepared using a spring-loaded venting apparatus as described previously.<sup>17</sup> Approximately 3 g of each of the  $\text{A}_n\text{B}_{n-1}\text{O}_{3n}$  phases were ground together with 4 molar equivalents of LiH and then heated for multiple periods of 3 days, with intermediate grinding.  $\text{Ba}_5\text{Nb}_4\text{O}_{15}$  was lithiated at 400°C,  $\text{Ba}_6\text{TiNb}_4\text{O}_{18}$  at 425°C and  $\text{Ba}_3\text{LaNb}_3\text{O}_{12}$  at 450°C. After the reactions were deemed complete, samples were washed with methanol under nitrogen to remove any remaining excess LiH, and then dried under vacuum.

Samples for magnetic analysis were washed for 2 hours in 5M HCl, to remove small amounts of ferromagnetic material (elemental iron) observed in magnetic data, but not in diffraction data, presumed to originate from the reduction apparatus. After this acid treatment, no decomposition of the materials was observed by X-ray diffraction.

Samples for transport measurements were prepared by taking 500 mg of the methanol-washed, lithiated materials and cold pressing this material into 13mm pellets under 5 tonnes force for 1 hour. The pressed pellets were then sealed in evacuated silica tubes and heated at 400°C for 7 days.

### Characterisation

X-ray powder diffraction data were recorded using a PANalytical X'Pert diffractometer incorporating an X'celerator position sensitive detector (monochromatic Cu K $\alpha$ 1 radiation). Samples containing LiH were measured in homemade air-tight sample holders sealed under an argon atmosphere. Neutron powder diffraction data were collected using the GEM diffractometer at the ISIS neutron source, UK, from samples contained in cylindrical vanadium cans. Rietveld profile refinements were performed using the GSAS suite of programs.<sup>18</sup> Magnetization data were collected using a Quantum Design MPMS SQUID magnetometer. Resistivity measurements were performed as a function of temperature using a 4-probe method on sample bars of known dimension cut from sintered pellets, prepared as described above.

## Results

### Chemical reactivity

Small test samples of  $\text{Ba}_5\text{Nb}_4\text{O}_{15}$ ,  $\text{Ba}_6\text{TiNb}_4\text{O}_{18}$  or  $\text{Ba}_3\text{LaNb}_3\text{O}_{12}$  mixed with LiH were observed to be unreactive

below 300 °C. Above this temperature these samples were observed to darken and there were significant changes to the powder X-ray diffraction patterns of samples. Raising reaction temperatures above 300 °C increased both reaction rates and the crystallinity of product phases. The optimum lithiation temperatures to produce the most crystalline materials were observed to be 400 °C for  $\text{Ba}_5\text{Nb}_4\text{O}_{15}$ , 425 °C for  $\text{Ba}_6\text{TiNb}_4\text{O}_{18}$  and 450 °C for  $\text{Ba}_3\text{LaNb}_3\text{O}_{12}$ . Above these reaction temperatures the crystallinity of materials was observed to decline and decomposition products, such as  $\text{LiNbO}_3$ , formed. Reactions between  $\text{Ba}_5\text{Ta}_4\text{O}_{15}$  and  $\text{LiH}$  followed a different pattern, with no evidence of lithiated materials being formed. At reaction temperatures below 400°C, no reaction was observed. Above these temperatures, reactions of  $\text{LiH}$  with  $\text{Ba}_5\text{Ta}_4\text{O}_{15}$  resulted in decomposition to form mixtures of the corresponding binary oxides and lithiated ternary oxides.

### Crystallographic characterisation

**$\text{Ba}_5\text{LiNb}_4\text{O}_{15}$ .** X-ray and neutron powder diffraction data collected from a lithiated sample of  $\text{Ba}_5\text{Nb}_4\text{O}_{15}$ , henceforth referred to as  $\text{Ba}_5\text{LiNb}_4\text{O}_{15}$ , can be indexed using a rhombohedral unit cell,  $a = 5.80 \text{ \AA}$ ,  $c = 35.67 \text{ \AA}$ . Compared to the unit cell of the primitive trigonal host phase,  $\text{Ba}_5\text{Nb}_4\text{O}_{15}$ ,<sup>13</sup> this corresponds to an approximate tripling of the  $c$ -lattice parameter on lithiation. The combination of symmetry change (primitive to rhombohedral) and geometric lattice expansion on lithiation is consistent with a ‘semi-topochemical’ reaction in which the  $-ccchh-$  stacking sequence of the  $\text{Ba}_5\text{Nb}_4\text{O}_{15}$  host phase is transformed into an entirely cubic stacking sequence, whilst the  $-\text{Nb}-\text{Nb}-\text{Nb}-\text{Nb}-\square-$  layered B-site ordering is retained. Thus a structural model was constructed in space group  $R\bar{3}m$  based on an entirely cubic stacking sequence, with an  $-\text{Nb}-\text{Nb}-\text{Nb}-\text{Nb}-\text{Li}-$  B-site layer ordering, as shown in Figure 1, and this model was refined against the neutron powder diffraction data. Close inspection of the diffraction data revealed a few weak features corresponding to a small quantity of the  $\text{Ba}_5\text{Nb}_4\text{O}_{15}$  starting material in the sample, so this was added as a second phase in the model. The refinement proceeded smoothly to give a good statistical fit, with all atomic positional and displacement parameters refining freely. In the final cycles of the refinement the occupancy parameters of the niobium and lithium B-cation sites were refined to probe the possibility of cation disorder or partial occupancy. The occupancies of all the B-cation sites refined to unity within error (error < 1%). Given the strong neutron scattering contrast between niobium and lithium ( $\text{Nb} = 7.05 \text{ fm}$ ;  $\text{Li} = -1.90 \text{ fm}$ )<sup>19</sup> this confirms the stated stoichiometry of the  $\text{Ba}_5\text{LiNb}_4\text{O}_{15}$  majority phase and confirms the presence of complete Li/Nb B-site cation order. Full details of the refined structure of  $\text{Ba}_5\text{LiNb}_4\text{O}_{15}$  are given in Table 1, with selected both lengths and plots of observed and calculated data given in the Supporting Information.

**$\text{Ba}_6\text{LiTiNb}_4\text{O}_{18}$ .** X-ray and neutron powder diffraction data collected from a lithiated sample of  $\text{Ba}_6\text{TiNb}_4\text{O}_{18}$ , henceforth referred to as  $\text{Ba}_6\text{LiTiNb}_4\text{O}_{18}$ , can be indexed using a primitive trigonal unit cell,  $a = 5.79 \text{ \AA}$ ,  $c = 14.25 \text{ \AA}$ . Compared to the unit

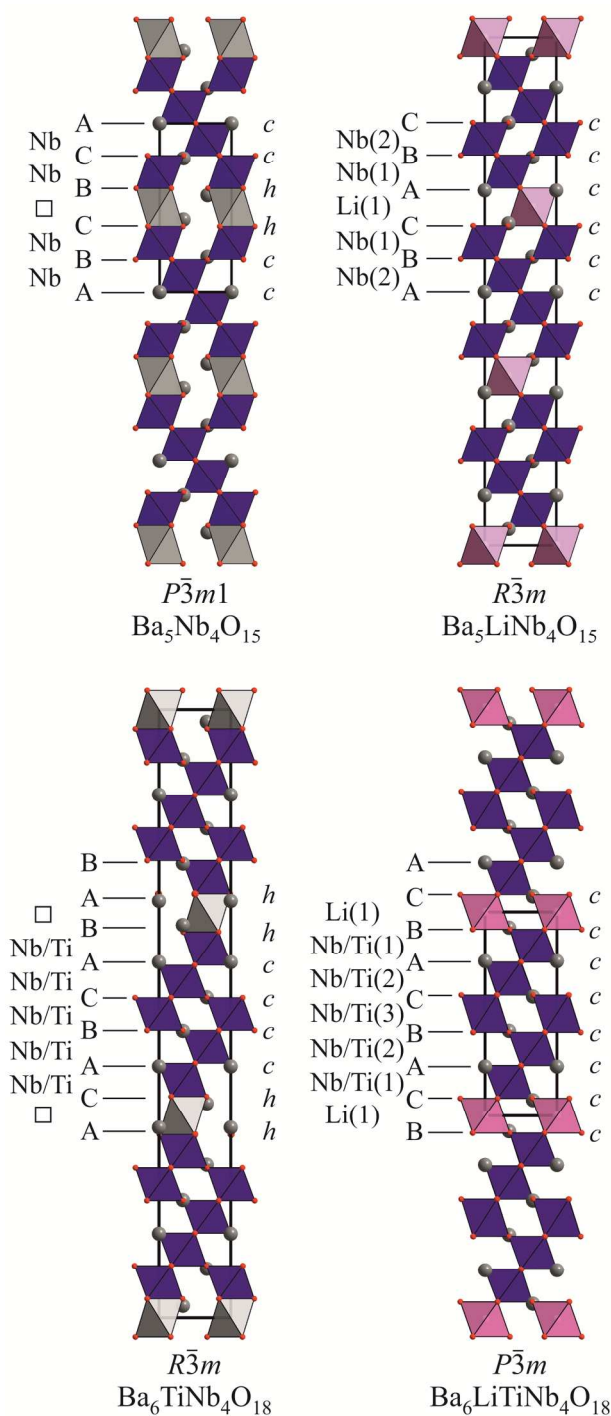


Figure 1: The crystal structures of  $\text{Ba}_5\text{Nb}_4\text{O}_{15}$ ,  $\text{Ba}_6\text{TiNb}_4\text{O}_{18}$  and their lithiated products  $\text{Ba}_5\text{LiNb}_4\text{O}_{15}$  and  $\text{Ba}_6\text{LiTiNb}_4\text{O}_{18}$ . Grey, red, blue and pink spheres represent barium, oxygen, niobium/titanium and lithium atoms respectively. The grey polyhedra indicate the position of the empty B-cations sites in  $\text{Ba}_5\text{Nb}_4\text{O}_{15}$  and  $\text{Ba}_6\text{TiNb}_4\text{O}_{18}$ .

cell of the rhombohedral host phase,  $\text{Ba}_6\text{TiNb}_4\text{O}_{18}$ ,<sup>14</sup> this corresponds to an approximate decrease by a factor of three of the  $c$ -lattice parameter on lithiation. The combination of symmetry change (rhombohedral to primitive) and geometric lattice contraction on lithiation is also consistent with a ‘semi-topochemical’ reaction in which the  $-ccchh-$  stacking sequence

Atom	x	y	z	U <sub>iso</sub> (Å <sup>2</sup> )
Ba(1)	2/3	1/3	0.0323(1)	0.0040(5)
Ba(2)	0	0	0.0979(1)	0.0050(7)
Ba(3)	1/3	2/3	1/6	0.0083(8)
Nb(1)	1/3	2/3	0.0646(1)	0.0037(5)
Nb(2)	2/3	1/3	0.1334(1)	0.0023(4)
Li(1)†	0	0	0	0.0016(8)
O(1)	0.1720(1)	0.3440(3)	0.0371(1)	0.0099(4)
O(2)	0.5002(1)	0.4997(1)	0.1021(1)	0.0063(5)
O(3)	5/6	2/3	1/6	0.0059(5)
Ba <sub>5</sub> LiNb <sub>4</sub> O <sub>15</sub> : space group <i>R</i> -3 <i>m</i> : <i>a</i> = 5.8012(3) Å, <i>c</i> = 35.675(2) Å Phase fraction: 90.2(3) weight percent				
Ba <sub>5</sub> Nb <sub>4</sub> O <sub>15</sub> : space group <i>P</i> -3 <i>m</i> 1: <i>a</i> = 5.7950(4) Å, <i>c</i> = 11.801(1) Å Phase fraction = 9.8(3) weight percent				
$\chi^2 = 4.085$ , wRp = 3.06%, Rp = 2.58%				

Table 1: Structural parameters of Ba<sub>5</sub>LiNb<sub>4</sub>O<sub>15</sub> refined from neutron powder diffraction data collected at 298K. †Refined lithium fractional occupancy = 1.00(1).

of Ba<sub>6</sub>TiNb<sub>4</sub>O<sub>18</sub> host phase is transformed into an entirely cubic stacking sequence, whilst B-site ordering of the lattice is retained, in a manner directly analogous to the observed during the lithiation of Ba<sub>5</sub>Nb<sub>4</sub>O<sub>15</sub>. Thus a structural model was constructed in space group *P*-3 based on an entirely cubic stacking sequence, with a Ti/Nb-Ti/Nb-Ti/Nb-Ti/Nb-Ti/Nb-Li B-site layer ordering, as shown in Figure 1, and this model was refined against the neutron diffraction data. The initial Ti/Nb distribution was set to that reported for the Ba<sub>6</sub>TiNb<sub>4</sub>O<sub>18</sub> host phase.<sup>14</sup> The refinement proceeded smoothly to give a good statistical fit, with all atomic positional parameters refining freely and atomic displacement parameters constrained by element to improve refinement stability. In the final cycles of the refinement the occupancy parameters of the niobium/titanium and lithium B-cation sites were refined to investigate the possibility of cation disorder and partially occupancy. The occupancy of the lithium site refined to unity within error (error < 1%) and the Ti/Nb distribution of the remaining B-cation sites refined to the values reported for the Ba<sub>6</sub>TiNb<sub>4</sub>O<sub>18</sub> starting phase within error. Given the neutron scattering length of titanium (-3.43 fm)<sup>19</sup> and the fact that each B-cation site could in principle contain a mixture of any of the three cations (Nb, Ti, Li), refinement of a model against a single data set cannot uniquely determine the cation distribution of Ba<sub>6</sub>LiTiNb<sub>4</sub>O<sub>18</sub>, even when the constraint that all the B-cation site must be fully occupied, is applied. Therefore in order to confirm the cation distribution in the material an identical model was refined against X-ray powder diffraction data collected from the sample. The refinement against X-ray powder diffraction data gave an almost identical cation distribution to that against the neutron powder diffraction data (deviations < 2%) and showed no evidence of titanium or niobium on the 'lithium' B-site. A simultaneous refinement against both X-ray and neutron powder diffraction data was not possible due to a slight mismatch in the observed lattice parameters in the two data sets (attributable to slightly different measuring temperatures) leading to significant increases in the error bars of many refined parameters when the model was

Atom	x	y	z	Fraction	U <sub>iso</sub> (Å <sup>2</sup> )
Ba(1)	0	0	0.2421(4)	1	0.0031(2)
Ba(2)	1/3	2/3	0.4162(5)	1	0.0031(2)
Ba(3)	2/3	1/3	0.0767(5)	1	0.0031(2)
Nb/Ti(1)	1/3	2/3	0.1642(3)	0.93/0.07	0.0019(1)
Nb/Ti(2)	2/3	1/3	0.3345(5)	0.72/0.28	0.0019(1)
Nb/Ti(3)	0	0	0.5	0.70/0.30	0.0019(1)
Li(1)	0	0	0	0.99(1)	0.0019(1)
O(1)	0.734(31)	0.3450(32)	0.0854(2)	1	0.0080(1)
O(2)	0.4981(22)	0.4927(22)	0.2470(2)	1	0.0080(1)
O(3)	0.8321(43)	0.1633(43)	0.4089(2)	1	0.0080(1)
Ba <sub>6</sub> LiTiNb <sub>4</sub> O <sub>18</sub> – space group <i>P</i> -3: <i>a</i> = 5.790(1) Å, <i>c</i> = 14.255(3) Å $\chi^2 = 5.043$ , wRp = 2.89%, Rp = 2.34%					

Table 2: Structural parameters of Ba<sub>6</sub>LiTiNb<sub>4</sub>O<sub>18</sub> refined from neutron powder diffraction data collected at 298K.

refined against both data sets simultaneously. Full details of the structure of Ba<sub>6</sub>LiTiNb<sub>4</sub>O<sub>18</sub> refined against the neutron diffraction data are given in Table 2, with selected bond lengths, plots of observed and calculated data from the refinement against neutron diffraction data, and details of the of the refinements against X-ray powder diffraction data, given in the Supporting Information. As can be seen in Table 2, the errors associated with the oxygen positional parameters in the refined structure of Ba<sub>6</sub>LiTiNb<sub>4</sub>O<sub>18</sub> are larger than equivalent errors in Ba<sub>5</sub>LiNb<sub>4</sub>O<sub>15</sub>. This is attributed to the presence of a disordered arrangement of niobium and titanium on the B-cation site of this phase.

**Ba<sub>3</sub>LaLiNb<sub>3</sub>O<sub>12</sub>.** X-ray and neutron powder diffraction data collected from a lithiated sample of Ba<sub>3</sub>LaNb<sub>3</sub>O<sub>12</sub>, henceforth referred to as Ba<sub>3</sub>LaLiNb<sub>3</sub>O<sub>12</sub>, can be indexed by a rhombohedral cell (*a* = 5.79 Å, *c* = 28.43 Å) with lattice parameters which are similar to those of the Ba<sub>3</sub>LaNb<sub>3</sub>O<sub>12</sub> starting material (*a* = 5.75 Å, *c* = 28.11 Å).<sup>15</sup> A model based on the structure of Ba<sub>3</sub>LaNb<sub>3</sub>O<sub>12</sub>, but with a lithium ion located on the vacant B-cation site, was therefore refined against the neutron powder diffraction data. The fit to the data with this model was poor, so the occupancies of the cations sites were refined (with the constraint that all cation sites were fully occupied) to investigate possible Ba/La A-site and Nb/Li B-site order/disorder. This led to a significant improvement to the fit and indicated that while the central B-cation site (Nb(3)) was fully occupied by niobium, the remaining Nb/Li(1) and Nb/Li(2) B-cation sites contained a disordered mixture of niobium and lithium (see Figure 2). In addition a strong preference for locating lanthanum on the A-cation sites located within cubic layers was observed. Close inspection of the data revealed a few weak features corresponding to a small quantity of the Ba<sub>3</sub>LaNb<sub>3</sub>O<sub>12</sub> starting material in the sample, so this was added as a second phase in the model. The refinement proceeded smoothly to give a good statistical fit, with all atomic positional parameters refining freely and atomic displacement parameters constrained by element to improve refinement stability. Full details of the refined structure of Ba<sub>3</sub>LaLiNb<sub>3</sub>O<sub>12</sub> are given in Table 3, with a representation of the structure of Ba<sub>3</sub>LaLiNb<sub>3</sub>O<sub>12</sub> given in Figure 2. Selected bond lengths and plots of observed and calculated data are given in the Supporting Information. In common with the

Atom	<i>x</i>	<i>y</i>	<i>z</i>	Fraction	<i>U</i> <sub>iso</sub> (Å <sup>2</sup> )
Ba/La(1)	0	0	0.2834(1)	0.60(1)/ 0.40(1)	0.0105(5)
Ba/La(2)	0	0	0.1335(2)	0.90(1)/ 0.10(1)	0.0105(5)
Nb/Li(1)	0	0	0.4165(1)	0.786(3)/ 0.214(3)	0.0068(6)
Nb/Li(2)	0	0	0.5	0.429(7)/ 0.571(7)	0.0068(6)
Nb(3)	0	0	0	1	0.0038(6)
O(1)	0.1690(5)	0.8309(5)	0.6283(1)	1	0.0208(6)
O(2)	0.1639(3)	0.8360(3)	0.4529(1)	1	0.0208(6)
Ba <sub>3</sub> LaLiNb <sub>3</sub> O <sub>12</sub> – space group <i>R</i> - $\bar{3}m$ : <i>a</i> = 5.7926(9) Å, <i>c</i> = 28.439(4) Å Phase fraction: 88.2(5) weight percent					
Ba <sub>3</sub> LaNb <sub>3</sub> O <sub>12</sub> – space group <i>R</i> - $\bar{3}m$ : <i>a</i> = 5.763(1) Å, <i>c</i> = 28.160(5) Å Phase fraction: 11.8(5) weight percent					
$\chi^2 = 1.265$ , wRp = 1.99%, Rp = 1.82%					

Table 3: Structural parameters of Ba<sub>3</sub>LaLiNb<sub>3</sub>O<sub>12</sub> refined from neutron powder diffraction data collected at 298K.

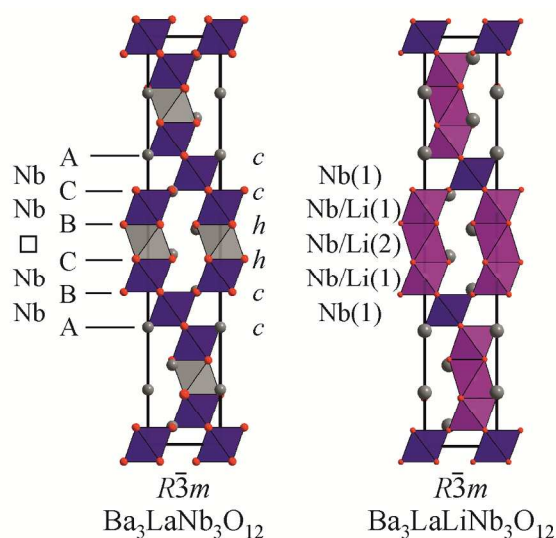


Figure 2: The structures of Ba<sub>3</sub>LaNb<sub>3</sub>O<sub>12</sub> and Ba<sub>3</sub>LaLiNb<sub>3</sub>O<sub>12</sub>. Grey, red, blue and purple spheres represent barium/lanthanum, oxygen, niobium and niobium/lithium positions respectively. The grey polyhedra indicate the position of the empty B-cations sites in Ba<sub>3</sub>LaNb<sub>3</sub>O<sub>12</sub>.

structural refinement of Ba<sub>6</sub>LiTiNb<sub>4</sub>O<sub>18</sub>, the structure of Ba<sub>3</sub>LaLiNb<sub>3</sub>O<sub>12</sub> was also refined against X-ray powder diffraction data to confirm the cation distributions in the material. As shown in the Supporting information, the cation distributions in this refinement do not deviate by more than 2%, confirming the refined structures. Full details of the refinement of Ba<sub>3</sub>LaLiNb<sub>3</sub>O<sub>12</sub> against X-ray powder diffraction data are given in the Supporting Information.

### Physical characterisation

Magnetisation data collected from Ba<sub>5</sub>LiNb<sub>4</sub>O<sub>15</sub>, Ba<sub>6</sub>LiTiNb<sub>4</sub>O<sub>18</sub> and Ba<sub>3</sub>LaLiNb<sub>3</sub>O<sub>12</sub> in an applied field of 1000 Oe, are shown in Figure 3. It can be seen that the magnetic susceptibility of all three phases shows only a small temperature dependence in the range 150 < T/K < 300. In the range 5 < T/K < 100 data collected from Ba<sub>6</sub>LiTiNb<sub>4</sub>O<sub>18</sub> and Ba<sub>3</sub>LaLiNb<sub>3</sub>O<sub>12</sub> can be fitted to the Curie-Weiss law, when a temperature independent term is included ( $\chi = C/(T-\theta) + K$ ), to

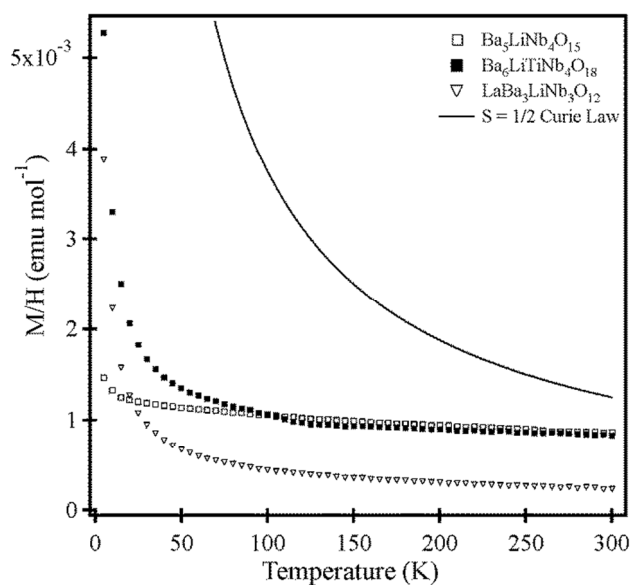


Figure 3: Magnetisation data collected from Ba<sub>5</sub>LiNb<sub>4</sub>O<sub>15</sub>, Ba<sub>6</sub>LiTiNb<sub>4</sub>O<sub>18</sub> and Ba<sub>3</sub>LaLiNb<sub>3</sub>O<sub>12</sub> as a function of temperature in an applied field of 1000 Oe. The solid line indicates the magnetic response expected for a simple *S* = 1/2 paramagnet obeying the Curie law.

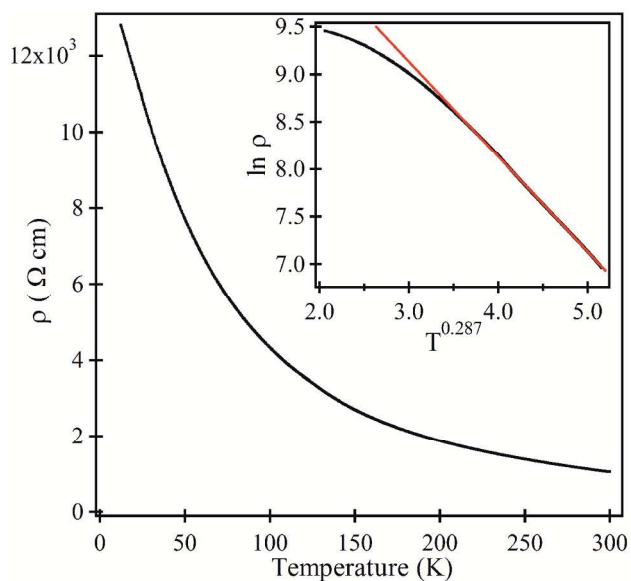


Figure 4: Resistivity data collected from Ba<sub>5</sub>LiNb<sub>4</sub>O<sub>15</sub> as a function of temperature. Inset shows plots of  $\ln \rho$  against  $T^{(1/3,49)}$  are linear for 70 < T/K < 300, consistent with variable range hopping behaviour.

yield values of  $C = 0.027 \text{ cm}^3 \text{ K mol}^{-1}$ ,  $\theta = -1.04 \text{ K}$ ,  $K = 8.1 \times 10^{-4} \text{ cm}^3 \text{ mol}^{-1}$  for Ba<sub>6</sub>LiTiNb<sub>4</sub>O<sub>18</sub> and  $C = 0.021 \text{ cm}^3 \text{ K mol}^{-1}$ ,  $\theta = -0.97 \text{ K}$ ,  $K = 2.2 \times 10^{-4} \text{ cm}^3 \text{ mol}^{-1}$  for Ba<sub>3</sub>LaLiNb<sub>3</sub>O<sub>12</sub>. The small size of the extracted Curie constants, and the observation that the temperature independent contribution to the magnetic susceptibility is almost identical to the 300 K susceptibilities for both Ba<sub>6</sub>LiTiNb<sub>4</sub>O<sub>18</sub> and Ba<sub>3</sub>LaLiNb<sub>3</sub>O<sub>12</sub>, are consistent with the presence of small quantities of paramagnetic impurities in these two samples. Thus the bulk magnetic response of all three lithiated phases is largely temperature independent over the whole measured temperature range.

4-probe DC resistivity data collected from  $\text{Ba}_5\text{LiNb}_4\text{O}_{15}$  as a function of temperature (Figure 4) indicate semiconducting behaviour. Fits to the data show they follow a  $T^{1/3}$ ,<sup>49</sup> temperature dependence, as shown in the inset to Figure 4, consistent with variable range hopping behaviour with a dimensionality reduced from fully three-dimensional, consistent with the layered nature of the phase which arises from the niobium/lithium cation order. We were not able to collect transport data from  $\text{Ba}_6\text{LiTiNb}_4\text{O}_{18}$  or  $\text{Ba}_3\text{LaLiNb}_3\text{O}_{12}$  due to the high resistivities of these phases ( $\rho > 10 \text{ K}\Omega \text{ cm}$  at 300 K).

## Discussion

Reaction of LiH with niobium-based, cation-deficient  $\text{A}_n\text{B}_{n-1}\text{O}_{3n}$  perovskite phases proceeds via reductive lithium insertion. These insertion reactions are rather unusual in that they only occur at elevated temperatures ( $T > 300 \text{ }^\circ\text{C}$ ). The need for elevated reaction temperatures can be attributed to the degree of structural rearrangement which occurs on lithium insertion – a change in the Ba-O lattice stacking in the case of  $\text{Ba}_5\text{Nb}_4\text{O}_{15}$  and  $\text{Ba}_6\text{TiNb}_4\text{O}_{18}$  and extensive niobium migration in the case of  $\text{Ba}_3\text{LaNb}_3\text{O}_{12}$ , as discussed in detail below. These structural changes can be seen to require ‘bond breaking’ and thus have high activation energies compared to the modest structural deformations which occur during the ambient temperature insertion of lithium into materials with rutile or  $\text{ReO}_3$ -type structures, for example.<sup>20, 21</sup> Indeed the lack of reactivity of  $\text{Ba}_5\text{Ta}_4\text{O}_{15}$  can also be attributed to the structural reorganisation required on reductive insertion of lithium, however in this case it appears that the stronger Ta-O bonds mean that the temperature required for the lattice rearrangement is comparable to the decomposition temperature of the phase and thus there is no temperature at which the lithium can be inserted into  $\text{Ba}_5\text{Ta}_4\text{O}_{15}$  to yield a metastable phase analogous to  $\text{Ba}_5\text{LiNb}_4\text{O}_{15}$ .

### Structural reorganisation on lithiation

As noted above, one of the most striking features of the lithium insertion into  $\text{A}_n\text{B}_{n-1}\text{O}_{3n}$  phases is the structural change which converts the *ccchh* and *cccchh* stacking sequences of  $\text{Ba}_5\text{Nb}_4\text{O}_{15}$  and  $\text{Ba}_6\text{TiNb}_4\text{O}_{18}$  respectively into entirely cubic stacking sequences in the lithiated phases (Figure 1). This structural change is reminiscent to ‘layer shift’ transformations seen during cation intercalation/deintercalation reactions in other extended oxides. For example on insertion of rubidium or caesium into  $\text{ALaNb}_2\text{O}_7$  ( $A = \text{Rb}, \text{Cs}$ ) Dion-Jacobson phases, the double sheets of  $\text{NbO}_6$  octahedra shift from a primitive to body-centred stacking arrangement resulting in the  $\text{A}_2\text{LaNb}_2\text{O}_7$  product phases adopting  $n = 2$  Ruddlesden-Popper structures.<sup>22, 23</sup> However in contrast to the distortion observed on lithiation of the Dion-Jacobson phases, which makes an additional coordination site for the inserted cations, the reason for the structural change on lithiation of  $\text{A}_n\text{B}_{n-1}\text{O}_{3n}$  phases is more subtle.

The structural changes observed on lithiation of  $\text{Ba}_5\text{Nb}_4\text{O}_{15}$  and  $\text{Ba}_6\text{TiNb}_4\text{O}_{18}$  can be understood by considering the structural

tolerance factor,  $t = \langle \text{A-O} \rangle / \sqrt{2} \langle \text{B-O} \rangle$ , which is commonly used to rationalise distortions in  $\text{ABO}_3$  perovskite phases. Phases with  $t = 1$  have an ideal ratio of A-O and B-O bond lengths to adopt an undistorted cubic perovskite structure in which  $\text{AO}_3$  layers are stacked in an ABCA cubic manner to yield an array of apex-linked  $\text{BO}_6$  octahedra. Phases with  $t < 1$  undergo twisting and tilting distortions of the apex-linked  $\text{BO}_6$  array which reduce the B-O-B bond angles from the ideal  $180^\circ$  angle to accommodate small A-cations. In contrast phases with  $t > 1$  tend to incorporate ABA hexagonal stacking into the sequence of  $\text{AO}_3$  layers which introduces face-sharing between  $\text{BO}_6$  octahedra, allowing larger A-cations to be accommodated. Considering the published structures of  $\text{Ba}_5\text{Nb}_4\text{O}_{15}$  and  $\text{Ba}_6\text{TiNb}_4\text{O}_{18}$  we can calculate tolerance factors of 1.016 and 1.012 for the two phases respectively from the experimentally determined bond lengths,<sup>13, 14</sup> consistent with the presence of hexagonal stacking in their structures. On lithium insertion we expect the B-cations will be reduced, leading to an increase in Nb-O bond lengths. In addition the 6-coordinate ionic radius of  $\text{Li}^+$  is larger than that of  $\text{Nb}^{5+}$  ( $\text{Li}^+ = 0.76 \text{ \AA}$ ,  $\text{Nb}^{5+} = 0.64 \text{ \AA}$ )<sup>24</sup>, thus a general increase in  $\langle \text{B-O} \rangle$  and decrease in the tolerance factor is expected on lithium intercalation, favouring all-cubic structures. The refined structures of  $\text{Ba}_5\text{LiNb}_4\text{O}_{15}$  and  $\text{Ba}_6\text{LiTiNb}_4\text{O}_{18}$  yield values of  $t = 0.990$  and  $t = 1.001$  respectively from the experimentally determined bond lengths, confirming the change in stacking sequence is attributable to the expected decline in tolerance factor on reductive lithium intercalation.

In contrast to the other  $\text{A}_n\text{B}_{n-1}\text{O}_{3n}$  phases,  $\text{Ba}_3\text{LaNb}_3\text{O}_{12}$  does not undergo any major structural rearrangement of the Ba-O framework on lithium insertion. Instead reaction with LiH inserts lithium into the  $\text{Ba}_3\text{LaNb}_3\text{O}_{12}$  framework in a fully topochemical manner, displacing some of the niobium cations from the Nb/Li(1) B-cation site, to yield a material with a disordered solid solution of Li/Nb on the Nb/Li(1) and Nb/Li(2) B-cation sites, as shown in Figure 2. Analysis of the refined structure of  $\text{Ba}_3\text{LaLiNb}_3\text{O}_{12}$  yields a tolerance factor of  $t = 1.010$ , consistent with the lack of a structural rearrangement and the retention of some hexagonal stacking in the Ba-O framework of the lithiated phase. However, it is hard to come to any definitive conclusions as to why a hexagonal structure is retained in  $\text{Ba}_3\text{LaLiNb}_3\text{O}_{12}$ , as direct comparisons between the structures of  $\text{Ba}_3\text{LaNb}_3\text{O}_{12}$  and  $\text{Ba}_3\text{LaLiNb}_3\text{O}_{12}$  are difficult because the only reported structure of  $\text{Ba}_3\text{LaNb}_3\text{O}_{12}$  was refined from X-ray powder diffraction data<sup>15</sup> and thus the locations of the oxide ions and the cation distribution reported for  $\text{Ba}_3\text{LaNb}_3\text{O}_{12}$  must be treated with caution.

### Physical behaviour and charge order

Magnetisation data collected from all three lithiated phases show positive susceptibilities (compared to the diamagnetic behaviour of the unlithiated starting materials) consistent with the partial reduction of the niobium/titanium centres. The approximate temperature independence of the susceptibilities of all three phases indicates that the electrons added on reduction

reside in extended bands, rather than on discrete paramagnetic transition metal cations. Transport data collected from all three samples indicate semiconducting ( $\text{Ba}_5\text{LiNb}_4\text{O}_{15}$ ) or insulating ( $\text{Ba}_6\text{LiTiNb}_4\text{O}_{18}$ ,  $\text{Ba}_3\text{LaNb}_3\text{O}_{12}$ ) behaviour. This indicates that the  $\pi^*$  electronic bands, formed predominately from the niobium 4d orbitals of  $t_{2g}$  symmetry, are narrow compared to the on-site electronic repulsion terms, as would be expected for an array of corner linked  $\text{MO}_6$  octahedra.

Considering the structural and physical data, the specific nature of the electronic localization appears to differ between the three lithiated phases. Resistivity data collected from  $\text{Ba}_5\text{LiNb}_4\text{O}_{15}$  exhibit a  $T^{1/3}$  temperature dependence (see inset to Figure 4) indicating variable range hopping behaviour. Taken with the magnetisation data this suggests  $\text{Ba}_5\text{LiNb}_4\text{O}_{15}$  is a small polaron conductor with localized  $\text{Nb}^{4+}$  centres and raises the further possibility of crystallographic charge order in the phase. Examining the structure of unlithiated  $\text{Ba}_5\text{Nb}_4\text{O}_{15}$  (as a non-charge ordered comparison phase) reveals that the bond valence sum (BVS)<sup>25</sup> values of the two crystallographically distinct niobium sites are significantly different (Nb(1) BVS = 5.09, Nb(2) BVS = +4.55).<sup>13</sup> Given that the oxidation state of all the niobium centres in  $\text{Ba}_5\text{Nb}_4\text{O}_{15}$  is unambiguously  $\text{Nb}^{5+}$  this difference in BVS value must be due to structural packing effects, such as the significant displacement of the Nb(1) centres towards the layer of vacant B-cations sites to minimise unfavourable Nb-Nb interactions. On lithium insertion to form  $\text{Ba}_5\text{LiNb}_4\text{O}_{15}$ , the BVS values of both niobium sites decline by approximately equal amounts (Nb(1) BVS = 4.72(3), Nb(2) BVS = +4.33(9)) providing no evidence for  $\text{Nb}^{4+}/\text{Nb}^{5+}$  charge ordering. Thus it appears that  $\text{Ba}_5\text{LiNb}_4\text{O}_{15}$  is a small polaron conductor with random dynamic localization of the 0.25 electrons per niobium added on lithium insertion.

In comparison the behaviour of  $\text{Ba}_6\text{LiTiNb}_4\text{O}_{18}$  is rather different. Analysis of the structure of unlithiated  $\text{Ba}_6\text{TiNb}_4\text{O}_{15}$  reveals that, in common with  $\text{Ba}_5\text{Nb}_4\text{O}_{15}$ , the three crystallographically distinct B-cation sites in the 6-layer phase have a range of BVS values (Nb(1) BVS = 4.75, Nb(2) BVS = +4.67, Nb(3) BVS = +4.52 – BVS values calculated as if all B-cation sites were fully occupied by Nb for simplicity).<sup>14</sup> However on lithiation the BVS value of the central Nb/Ti(3) site declines by a much larger amount than the other two B-cation sites, even when the error bars are considered, (Nb(1) BVS = 4.54(9), Nb(2) BVS = +4.41(21), Nb(3) BVS = +3.52(22)) suggesting the electrons added into the framework on lithium insertion are localized as  $\text{Nb}^{4+}/\text{Ti}^{3+}$  centres on the Nb(3) cation site, with the remaining Nb/Ti(1) and Nb/Ti(2) sites containing  $\text{Nb}^{5+}/\text{Ti}^{4+}$  cations. This crystallographic charge order will exert a much higher barrier to ‘electron hopping’ than the disordered charge localization observed for  $\text{Ba}_5\text{LiNb}_4\text{O}_{15}$ , accounting for the much greater resistivity observed for  $\text{Ba}_6\text{LiTiNb}_4\text{O}_{18}$ .

Analysis of the structure of  $\text{Ba}_3\text{LaLiNb}_3\text{O}_{12}$  is complicated by the extensive niobium/lithium disorder. However detailed examination of the refined structure of  $\text{Ba}_3\text{LaLiNb}_3\text{O}_{12}$  shows that the B-cation site which is only occupied by niobium (Nb(3)) has a BVS value of Nb +5.01(1). This suggests that the

additional electrons added on lithium insertion are localized on the Nb/Li(1) and Nb/Li(2) sites, where the disordered array of lithium and niobium cations will reinforce the charge localization accounting for the high resistivity of this phase.

The transport behaviour observed for the  $\text{A}_n\text{LiB}_{n-1}\text{O}_{3n}$  phases is broadly consistent with that of other mixed valent Nb(IV)/Nb(V) perovskite phases. For example members of the  $\text{K}_{1-x}\text{Ba}_x\text{NbO}_3$  solid solution are observed to be semiconductors ( $dp/dT < 0$ ) for  $x \leq 0.5$ .<sup>26</sup> Likewise, phases in the  $\text{Na}_{1-x}\text{Sr}_x\text{NbO}_3$  solid solution are insulators for  $x < 0.3$  and semiconducting for  $x = 0.3$  and  $0.4$ , with a change to metallic behaviour at  $x = 0.5$ .<sup>27</sup> These observations combined with the data in this study suggest the niobium 4d  $\pi^*$  bands are too narrow to allow metallic conductivity at low d-electron counts.

## Conclusions

Lithium insertion into niobium based  $\text{A}_n\text{B}_{n-1}\text{O}_{3n}$  perovskite phases readily yields topochemically reduced, mixed valent Nb(IV)/Nb(V) perovskite oxides. The insertion of lithium appears to be stoichiometric, thus the oxidation state of niobium in the lithiated phase is defined by the level of cation deficiency in the lattice of the original material. This feature of the reactions suggest this method could be a powerful method for preparing metastable perovskite phases with transition metals in well-defined, but unusually low, oxidation states.

## Acknowledgements

We thank W. Kockelmann and I. da Silva for assistance collecting the neutron powder diffraction data. Experiments at the ISIS pulsed neutron facility were supported by a beam time allocation from the Science and Technology Facilities Council. A.P. acknowledges financial support from project CTQ2011-27626 (Spanish Ministerio de Economía y Competitividad), Junta de Andalucía (TEP-7858) and FEDER funds.

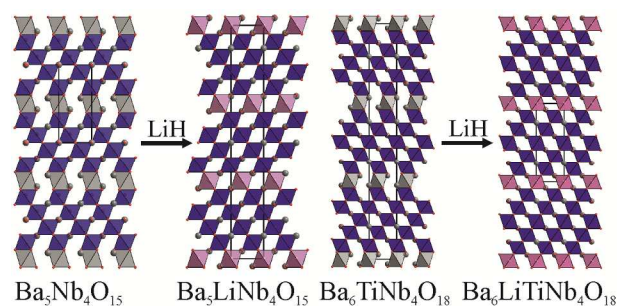
## Notes and references

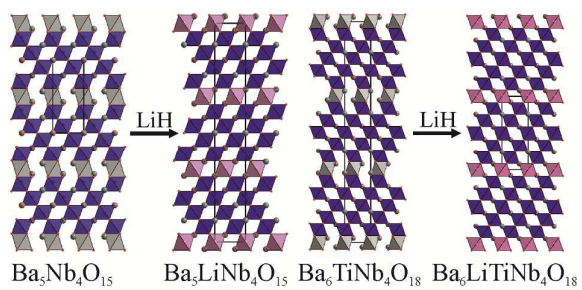
<sup>a</sup> Department of Chemistry, University of Oxford, Inorganic Chemistry Laboratory, South Parks Road, Oxford, OX1 3QR, United Kingdom. Fax: +44 1865 272600; Tel: +44 1865 272623; E-mail: michael.hayward@chem.ox.ac.uk  
Electronic Supplementary Information (ESI) available: Selected bond lengths and plots of observed and calculated data from the refinements against neutron powder diffraction data of  $\text{Ba}_5\text{LiNb}_4\text{O}_{15}$ ,  $\text{Ba}_6\text{LiTiNb}_4\text{O}_{18}$  and  $\text{Ba}_3\text{LaLiNb}_3\text{O}_{12}$ . Full details and plots of observed and calculated data from the refinement of  $\text{Ba}_6\text{LiTiNb}_4\text{O}_{18}$  and  $\text{Ba}_3\text{LaLiNb}_3\text{O}_{12}$  against X-ray powder diffraction data. See DOI: 10.1039/b000000x/

1. J. G. Bednorz and K. A. Müller, *Z. Phys. B*, 1986, **64**, 189-193.
2. C. N. R. Rao and B. Raveau, eds., *Colossal Magnetoresistance, Charge Ordering and Related Properties of Manganese Oxides*, World Scientific, Singapore, 1998.
3. J. B. Goodenough and J.-S. Zhou, *Chem. Mater.*, 1998, **10**, 2980-2993.
4. J. B. Goodenough, ed., *Localized to Itinerant Electronic Transition in Perovskite Oxides*, Springer-Verlag, Berlin, 2001.

5. M. A. Hayward, M. A. Green, M. J. Rosseinsky and J. Sloan, *J. Am. Chem. Soc.*, 1999, **121**, 8843-8854.
6. J. Seddon, E. Suard and M. A. Hayward, *J. Am. Chem. Soc.*, 2010, **132**, 2802-2810.
7. Y. Tsujimoto, C. Tassel, N. Hayashi, T. Watanabe, H. Kageyama, K. Yoshimura, M. Takano, M. Ceretti, C. Ritter and W. Paulus, *Nature*, 2007, **450**, 1062-1065.
8. F. Denis Romero, S. J. Burr, J. E. McGrady, D. Gianolio, G. Cibirin and M. A. Hayward, *J. Am. Chem. Soc.*, 2012, **135**, 1838.
9. E. Dixon, J. Hadermann, S. Ramos, A. L. Goodwin and M. A. Hayward, *J. Am. Chem. Soc.*, 2011, **133**, 18397.
10. D. W. Murphy, F. J. Disalvo, J. N. Carides and J. V. Waszczak, *Mater. Res. Bull.*, 1978, **13**, 1395-1402.
11. D. E. Cox, R. J. Cava, D. B. McWhan and D. W. Murphy, *J. Phys. Chem. Solids*, 1982, **43**, 657-666.
12. I. J. Davidson and J. E. Greedan, *J. Solid State Chem.*, 1984, **51**, 104-117.
13. S. Pagola, G. Polla, G. Leyva, M. T. Casais, J. A. Alonso, I. Rasines and R. E. Carbonio, in *European Powder Diffraction: Epcid Iv, Pts 1 and 2*, 1996, vol. 228, pp. 819-824.
14. H. C. Van Duivenboden, H. W. Zandbergen and D. J. W. Ijdo, *Acta Crystallographica Section C-Crystal Structure Communications*, 1986, **42**, 266-268.
15. H. J. Rother, S. Kemmlersack, U. Treiber and W. R. Cyris, *Z. Anorg. Allg. Chem.*, 1980, **466**, 131-138.
16. N. Harre, D. Mercurio, G. Trolliard and B. Frit, *Mater. Res. Bull.*, 1998, **33**, 1537-1548.
17. M. O'Malley, M. A. Lockett and M. A. Hayward, *Journal of Solid State Chemistry*, 2007, **180**, 2851-2858.
18. A. C. Larson and R. B. Von Dreele, Los Alamos National Laboratory Report LAUR 86-748, 2000.
19. V. F. Sears, *Neutron News*, 1992, **3**, 26-37.
20. R. J. Cava, A. Santoro, D. W. Murphy, S. Zahurak and R. S. Roth, *J. Solid State Chem.*, 1982, **42**, 251-262.
21. K. H. Cheng and M. S. Whittingham, *Solid State Ionics*, 1980, **1**, 151-161.
22. A. R. Armstrong and P. A. Anderson, *Inorg. Chem.*, 1994, **33**, 4366-4369.
23. J. Choi, X. Zhang and J. B. Wiley, *Inorg. Chem.*, 2009, **48**, 4811-4816.
24. R. D. Shannon, *Acta Cryst.*, 1976, **A32**, 751.
25. N. E. Brese and M. O'Keeffe, *Acta Crystallogr., Sect. B: Struct. Sci.*, 1991, **B47**, 192-197.
26. E. M. Kopnin, S. Y. Istomin, O. G. Dyachenko, E. V. Antipov, P. Bordet, J. J. Capponi, C. Chaillout, M. Marezio, S. Debrion and B. Souletie, *Mater. Res. Bull.*, 1995, **30**, 1379-1386.
27. S. Y. Istomin, G. Svensson and J. Kohler, *J. Solid State Chem.*, 2002, **167**, 7-16.

TOC figure





Reductive lithium intercalation into  $\text{A}_n\text{B}_{n-1}\text{O}_{3n}$  cation deficient perovskite phases leadsto the formation of  $\text{Ba}_5\text{LiNb}_4\text{O}_{15}$ ,  $\text{Ba}_6\text{LiTiNb}_4\text{O}_{18}$  and  $\text{Ba}_3\text{LaLiNb}_3\text{O}_{12}$ .